CRYSTAL STRUCTURE HIRSHFELD SURFACE AND COMPUTATIONAL ANALYSIS OF 4-CHLOROPHENYL BENZIMIDAZOLE AND 3-CHLOROPHENYL BENZOTHIAZOLE

F. ODAME*, A. S. K. AMABLE, F. ACHEAMPONG
Department of Basic Sciences, University of Health and Allied Sciences, PMB 31, Ho, Ghana.
**Corresponding author's email address: felixessah15@gmail.com*

ABSTRACT

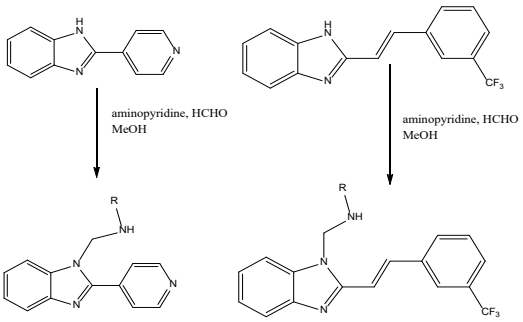
The crystal structures, Hirshfeld surface analysis, and computational studies of 4-chlorophenyl benzimidazole and 3-chlorophenyl benzothiazole have been presented. Compound **I** crystallized in the monoclinic space group *I2/a* whilst compound **II** crystallized in the orthorhombic space group *Pbca.* Both compounds had 8 molecules in their unit cells. The experimental and computed bond lengths and bond angles showed good agreement among the results with varying deviations from each other. Hirshfeld surface analysis of the compounds revealed that the most significant contributions to the crystal packing for compound **I** came from H···H (28.7%), H···C/C···H (26.5%), Cl···H (18.1%) and H···N/N···H (4.5%) whilst the atoms contributing to the crystal packing in compound **II** were H···H (34.5%), H···C/C···H (30.1%), Cl···H (12.5%) , H···N/N···H (10.2%), Cl···C (4.1%), Cl···N (1.9%) and Cl···Cl (2.1%). This work presents the first comparison of the computed and experimental bond parameters, Hirshfeld analysis and the HOMO-LUMO analysis of 4-chlorophenylbenzimidazole and 3-chlorophenylbenzothiazole, providing the basis for comparison of bulkier bioactive benzimidazole and benzothiazole derivatives.

Key words: benzothiazole, benzimidazole, Hirshfeld surface analysis

Introduction

Benzimidazole is a bicyclic molecule that is mostly produced by condensing *o*-phenylenediamine with aldehydes or carboxylic acids. The have be reported to have a variety of biological and therapeutic effects. They have been synthesized by a variety of methods and have been reported to exhibit different biological activities[1-3]. Some have been found to be active against gram negative bacteria[1], whilst others are antimicrobial, antituberculosis and antiprotozoal [2], antitumor, diuretic, fungicidal, bactericidal, antihelmintic, antiallergic, antihistaminic, vasodilator, hypotensive, spasmolytic activities and local analgesic properties [3]. Scheme 1 gives the scheme for the synthesis of some *N*-substituted benzimidazole derivatives

GJS is an Open Access Journal and distributed under the terms of Creative Commons (CC) License [CC by 4.0]



Scheme 1 Synthesis of *N*-substituted benzimidazole derivatives

Some benizimidazole containimg compounds have been found to exhibit good activity against *Mycobacterium tuberculosis* [4]. Different benzothiazole derivatives have been accessed by different methods [4-5], including by microwave irradiation [5], and by using a base together with a coupling agent [6]. Benzothiazoles have been found to be active against gram-positive and gram negative bacteria[7,] and also as antifungal agents [8]. Some benzimidazole, benzoxazole and benzothiazole derivatives have been accessed from aromatic aldehydes with *o*-phenylene diamine, *o*-amino phenol and *o*-amino thiophenol [9]. Benzothiazole, benzoxazole and benzimidazole derivatives have been reported to exhibit good anti-tumor activities.[10]. Benzothiazole derivatives have been reported to exhibit a variety of pharmacological activities including antitumor, antimicrobial, anti-inflammatory, anticonvulsant, and antidiabetic activities. It is a versatile scaffold that has found use in many drugs [11].

We herein report, the crystal structures, Hirshfeld surface analysis and computational studies of 4-chlorophenyl benzimidazole and 3-chlorophenyl benzothiazole. A discussion on the single crystal XRD data of the compounds have been presented to provide insights into the structural properties of these compounds. The computed and experimental bond lengths, bond angles and the Hirshfeld surface analysis of the compounds have been discussed to show how the structural properties of these compounds can be exploited to develop compounds that have enhanced properties for different biological targets.

Experimental

Materials and physical measurements

Analytical grade reagents and solvents for synthesis such as *o*-phenylenediamine, 2-chlorobenzaldehyde, Bismuth nitrate pentahydrate and 4-methylpent-3-en-2-one were obtained from Sigma Aldrich (USA) whilst ethanol, acetone and ethanol were obtained from Merck Chemicals (SA). The reagents were used without any further purification. The reaction was followed with TLC using ethyl acetate: petroleum ether (1:1). ^{1}H NMR and ^{13}C NMR spectra were recorded on a Bruker Avance AV 400-MHz spectrometer operating at 400MHz for ^{1}H and 100M Hz for ^{13}C using dimethylsulfoxide as solvent and tetramethylsilane as internal standard. Chemical shifts are expressed in ppm. FT-IR spectra were recorded on a Bruker Platinum ATR Spectrophotometer Tensor 27. Microanalysis was performed using a Vario Elementar Microcube ELIII. Melting points were obtained using a Stuart Lasec SMP30 and were reported uncorrected, while the masses were determined using a PerkinElmer GC Clarus 580 Gas Chromatograph interfaced to a Mass Spectrometer PerkinElmer (Clarus SQ 8 S) equipped with ZB-5HTMS (5% diphenyl/95% dimethyl polysiloxane) fused capillary column (30 × 0.25-µm ID×0.25-µm DF). The oven temperature was programmed from 100 °C (isothermal for 2 min), with an increase of 10 °C/min to 200 °C, then 5 °C/min to 280 °C, and holding for 6 mins

at 280 °C. For gas chromatography–mass spectrometry (GC–MS) detection, an electron ionization system was operated in electron-impact mode with ionization energy of 70 eV. Helium gas (99.9999%) was used as a carrier gas at a constant flow rate of 1 mL/min, and an injection volume of 1 µL was employed. The injector temperature was maintained at 250 °C, the ion-source temperature was 220 °C. Mass spectra were taken at 70 eV; a scan-interval of 1 s and fragments from 50 to 500 Da. The solvent delay was 0–3min, and the total GC/MS running time was 50 min, respectively. The mass detector used in this analysis was Turbo-Mass, and the software adopted to handle mass spectra and chromatograms was Turbo-Mass ver-6.1.0. Interpretation on mass spectrum GC–MS was conducted using the database of the National Institute of Standard and Technology (NIST) having more than 62,000 patterns.

2-(3-chlorophenyl)-1,3-benzothiazole **(I)**

10% Bismuth nitrate pentahydrate was placed in 20 mL of ethanol, 2-aminothiophenol (0.03 mol, 3.76 g) and 3-chlorobenzaldehyde (0.03 mol, 4.22 g) were added and stirred for 4 h at room temperature. The reaction mixture was decanted to remove the residual catalyst and allowed to stand overnight in the fume hood, to produce the impure products as the solvent evaporated. The product was recrystallized and obtained as a brown solid from ethanol:acetone (1:1). Yield = 78%, Mp = 98–99 °C. ^{1}H NMR (ppm): 8.12 (d, *J* = 8.0 Hz, 1H), 8.06 (m, 2H), 8.06 (d, *J* = 7.2 Hz, 1H), 7.60 (t, *J* = 8.0 Hz, 1H), 7.56 (q, *J* = 7.2, 7.6 Hz, 2H), 7.47 (t, *J* = 7.6 Hz, 1H). ^{13}C NMR (ppm): 166.2 (C=N), 153.8 (C), 135.2 (C), 134.7 (C), 131.7 (C), 127.1 (CH), 126.8 (CH), 123.7 (CH), 122.9 (CH). IR (ν_{max}, cm^{-1}): 2981(C-H), 2112, 1568 (C=N), 1500 (C=C), 1457 (C–N). Anal.calcd. for $C_{13}H_8ClNS$: C, 63.54; H, 3.28; S, 13.05; N, 5.70. Found: C, 63.48; H, 3.34; S, 13.00; N, 5.62. LRMS (*m/z*, M^{+}): Found for $C_{13}H_8ClNS$ = 245.67, Expected mass = 245.73.

2-(4-chlorophenyl)-1H-benzimidazole **(II)**

10% Bismuth nitrate pentahydrate was dissolved in 20 mL ethanol, *o*-phenylenediamine (0.03 mol, 3.24 g) and 4-chlorobenzaldehyde (0.03 mol, 4.22 g) were added stirred for 4 h at room temperature. The reaction mixture was decanted to remove the residual catalyst and allowed to stand overnight in the fume hood, to produce the impure products as the solvent evaporated. The product was recrystallized and obtained as a brown solid from ethanol:acetone (1:1) Yield = 80 %, Mp = 289–291 °C. ^{1}H NMR (ppm): 12.98 (s, 1H), 8.20 (d, J = 8.4 Hz, 2H), 7.64 (t, J = 8.4 Hz, 3H), 7.55 (s, 2H), 7.22 (s, 2H). ^{13}C NMR (ppm): 150.5, 134.8, 129.5, 128.6, 123.2, 122.3, 119.4, 111.8. IR (νmax, cm^{-1}): 3052, 2848, 1587, 1472, 1448, 1397, 1372, 1321, 1273, 1226. Anal.calcd. for $C_{13}H_9N_2Cl$: C, 68.75; H, 3.97; N, 12.25. Found: C, 68.61; H, 4.03; N, 12.31. LRMS (m/z, M+): Found for $C_{13}H_9N_2Cl$ = 228.55, Expected mass = 228.68.

X-ray crystallography

X-ray diffraction analysis of 2-(3-chlorophenyl)-1,3-benzothiazole (**I**) and 2-(4-chlorophenyl)-1H-benzimidazole (**II**) were performed at 200 K using a Bruker Kappa Apex II diffractometer with monochromated Mo Kα radiation (λ = 0.71073 Å). APEXII, [12] was used for data collection and SAINT, [12] for cell refinement and data reduction. The structures were solved by direct methods using SHELXS–2013 [12], and refined by least-squares procedures using SHELXL-2013, [13] with SHELXLE, [14] as a graphical interface. All non-hydrogen atoms were refined anisotropically. Carbon-bound H atoms were placed in calculated positions (C–H 0.95 Å for aromatic

carbon atoms and C–H 0.99 Å for methylene groups) and were included in the refinement in the riding model approximation, with U_{iso} (H) set to $1.2U_{eq}$ (C). The H atoms of the methyl groups were allowed to rotate with a fixed angle around the C–C bond to best fit the experimental electron density (HFIX 137 in the SHELX program suite (Sheldrick, 2008), with U_{iso} (H) set to $1.5U_{eq}$ (C). Nitrogen-bound H atoms were located on a difference Fourier map and refined freely. Data were corrected for absorption effects using the numerical method implemented in SADABS [14].

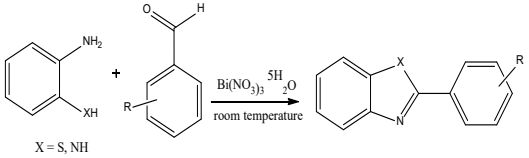
Computational studies

Gaussian 09 program was used for all the calculations. The structures were fully optimized at the singlet ground state in the gas phase using the density functional theory (DFT). The functionals used for computation were the B3LYP, B3PW91, WB97XD and M06 functionals and 6-311g(d, p) basis set. The choice of functional used was based on work reported in literature [15-18]. Optimization and frequency calculations were carried out to ensure that the optimized molecular structures corresponded to a minimum. The results were viewed in Avogadro or Gaussview 6.0.

Results and discussion

Optimization of synthetic method.

The compounds were recrystallized from ethanol:acetone (1:1) as a brown solid crystals. **Scheme 2** gives the reaction scheme for the synthesis of the benzothiazole and benzimidazole derivative.



Scheme 2 Reaction scheme for benzothiazoles and benzimidale derivatives.

X-ray crystal structures of compounds **I** and **II** were obtained using single crystals grown by crystallization. **Table 1** and **2** shows the crystallographic data, selected bond lengths and bond angles for the crystal structures of compounds **I** and **II**. Compound **I** was recrystallized from ethanol:acetone (1:1) and obtained as a brown solid. It re-crystallized in the monoclinic space group *I2/a*. **Figure 1** gives the ORTEP diagram for compound **I** whilst the ORTEP diagram of compound **II** which was recrystallized from ethanol:acetone (1:1) and obtained as a bown solid is given by **Figure 2**. Compound **II** crystallized in the orthorhombic space group *Pbca.* The bond distances of S1-C1 and S1-C22 in compound **I** which were 1.751(2) and 1.728(1) Å, respectively were consistent with the thione bond, whilst the bond distances of N1-C1 and N1-C21 were 1.299(2) and 1.386(2) Å respectively. The bond distances of C1-C11 and C11-C12 were 1.468(2) and 1.392(2) Å respectively.

TABLE 1

*Crystallographic data and structure refinement summary for compounds **I** and **II***

Property	**Compound I**	**Compound II**
Formula	$C_{13}H_8ClNS$	$C_{13}H_9ClN_2$
CCDC	1528309	1528306
Formula Weight	245.71	228.67
Crystal System	Monoclinic	orthorhombic
Space group	*I2/a*	*Pbca*
a [Å]	16.5507(11)	9.1475(3)
b [Å]	5.7730(4)	9.7503(3)
c [Å]	23.2480(15)	23.8121(8)
α [°]	90	90
β [°]	99.734(4)	90
γ [°]	90	90
V [Å^3]	2189.3(3)	2123.82(12)
Z	8	8
D(calc) [g/cm^3]	1.491	1.43
Mu(MoKa) [/mm]	0.506	0.329
F(000)	1008	944
Crystal Size [mm]	0.28 x 0.31 x 0.66	0.10 x 0.12 x 0.53
Temperature (K)	200	200
Radiation [Å]	MoKa 0.71073	MoKa 0.71073
Theta Min-Max [°]	2.5, 28.3	2.8, 28.3
Dataset	-22: 21 ; -7: 7 ; -31: 31	-12: 12 ; -13: 13 ; -30: 30
Tot., Uniq. Data, R(int)	18576, 2718, 0.015	45214, 2631, 0.023
Observed Data [I > 2.0 sigma(I)]	2459	2291
Nref,	2718	2631
Npar	145	149
R	0.0303	0.0375
$_wR_2$	0.0811	0.0970
S	1.04	1.04
Max. and Av. Shift/Error	0.00, 0.00	0.00, 0.00
Min. and Max. Resd. Dens. [e/Å^3]	-0.33	-0.26
Min. and Max. Resd. Dens. [e/Å^3]	0.33	0.34

The bond angles of N1-C1-C11, N1-C21-C22 and N1-C21-C26 were 123.4(1), 115.00(1) and 125.1(1)° respectively whilst the S1-C22-C21 and S1-C22-C23 bond angles were 109.5(1) and 129.1(1)° respectively. The bond angles of C1-S1-C22, S1-C1-N1 and S1-C1-C11 were 89.1(1), 115.00(1) and 120.7(1)° respectively In compound **II**, the bond distances of N1-C1, N1-C11, N2-C1 and N2-C12 which were 1.328(2), 1.393(2), 1.362(2) and 1.376(2) Å, and consistent with the C-N single bond, [15] respectively, whilst the Cl-C24 and C21-C22 bond distances in compound **II** were 1.738(1) and 1.390(2) Å respectively . The bond distances of C22-C23, C11-C12 were 1.381(2) and 1.406 (2). The bond angles of C1-N1-C11, C1-N2-C12, and N1-C1-N2 in compound **II** were 104.8 (1), 107.2(1), and 112.9(1)° respectively. Whilst the N1-C1-C21, N2-C1-C21, and N1-C11-C16 bond angles were 125.1(1), 122.0(1), and 130.8(1)° respectively. The bond angles of N1-C11-C12, N2-C12-C13 and N2-C12-C11 were 109.5(1) 132.0(1) and 105.6(1)°.

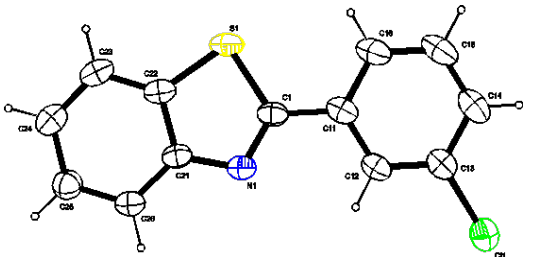


Fig.1**:** An ORTEP view of 2-(3-chlorophenyl)-1,3-benzothiazole (**I**) showing 50% probability displacement ellipsoids and the atom labelling.

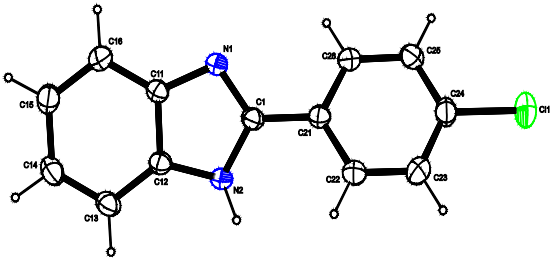


Fig.2: An ORTEP view of 2-(4-chlorophenyl)-1H-benzimidazole (**II**) showing 50% probability displacement ellipsoids and the atom labelling.

Comparison of theoretical and experimental bond parameters

Table 2 gives the summary of theoretical and experimental bond lengths and bond angles for compound **I** using B3LYP, B3PW91, WB97XD and M06 functionals and 6-311g (d,p) basis set. The bond lengths of Cl1-C13, C1-C11, C11-C12 and C11-C16 was experimentally determined as 1.509(1), 1.468(2), 1.392(2) and 1.397(2) Å, whilst the computed bond lengths gave deviations between 0.030 and 0.158 Å from the experimental values. For the amide bonds N1-C1 and N1-C21 the experimental bond lengths obtained were 1.299(2) and 1.386(2) Å, respectively, the computed values deviated by 0.008 and 0.095 Å. The bond lengths of S1-C1 and S1-C22 were experimentally determined as 1.751(2) and 1.728(1) Å whilst the computed values gave deviations between 0.012 and 0.026 Å. The bond angles of N1-C1-C11, N1-C21-C22 and N1-C21-C26 were experimentally determined as 123.4(1), 115.00(1) and 125.1(1)° with deviations between 0.40 and 2.2° for the computed values.

TABLE 2

*Summary of theoretical and experimental bond lengths (Å), and bond angles (°) for 2-(3-chlorophenyl)-1,3-benzothiazole (**I**) using B3LYP, CAM-B3LYP, B3PW91, WB97XD and M06 functionals and 6-311g(d,p) basis set.*

Bond length (Å) Compound I							
Experimental		**B3LYP**	**B3PW91**	**WB97XD**	**M06**	**Min Deviation**	**Max Deviation**
Cl1-C13	1.740(1)	1.703	1.692	1.700	1.692	0.037	0.048
S1-C1	1.751(2)	1.775	1.764	1.768	1.773	0.013	0.024
S1-C22	1.728(1)	1.716	1.709	1.702	1.707	0.012	0.026
N1-C1	1.299(2)	1.307	1.367	1.382	1.363	0.008	0.083
N1-C21	1.386(2)	1.370	1.305	1.291	1.301	0.016	0.095
C1-C11	1.468(2)	1.403	1.402	1.381	1.394	0.065	0.158

C11-C12	1.392(2)	1.430	1.425	1.441	1.425	0.030	0.049
C11-C16	1.397(2)	1.453	1.450	1.447	1.445	0.048	0.056
C12-C13	1.383(2)	1.377	1.376	1.370	1.371	0.006	0.013

Bond Angles (°)							
Experimental		**B3LYP**	**B3PW91**	**WB97XD**	**M06**	**Min Deviation**	**Max Deviation**
C1-S1-C22	89.1(1)	89.0	89.0	89.2	88.6	0.1	0.5
C1-N1-C21	110.6(1)	111.6	111.2	111.3	111.3	0.6	1.0
S1-C1-N1	115.8(1)	114.4	114.8	114.2	114.8	1.0	1.6
S1-C1-C11	120.7(1)	124.2	123.9	124.5	123.5	2.8	3.8
N1-C1-C11	123.4(1)	121.2	121.9	121.3	121.7	1.5	2.2
N1-C21-C22	115.00(1)	115.4	115.4	115.6	115.5	0.4	0.6
N1-C21-C26	125.1(1)	124.5	124.4	124.3	124.5	0.6	0.8
S1-C22-C21	109.5(1)	109.6	109.6	109.7	109.8	0.1	0.3
S1-C22-C23	129.1(1)	129.8	129.7	129.7	129.4	0.3	0.7

The bond angles of S1-C22-C21, S1-C22-C23 and S1-C1-C11 were experimentally determined as 109.5(1), 129.1(1) and 120.7(1)° with deviations between 0.1 and 3.8° representing the lowest and largest deviations, respectively, from the experimental values. The bond angles of C1-S1-C22, C1-N1-C21 and S1-C1-N1 were experimentally determined as 89.1(1) 110.6(1) and 115.8(1)°, whilst the computed values gave deviations between 0.1 and 1.6° from the experimental values. In compound **II t**he bond length of the amide bonds N1-C1, N1-C11, N2-C1 and N2-C12 were experimentally determined as 1.328(2), 1.393(2), 1.362(2) and 1.376(2) Å, whilst the computed bond length gave deviations between 0.003 and 0.033Å from the experimental values. The bond length of C1-C21, C22-C23 and C11-C12 was experimentally determined as 1.466(2), 1.381(2) and 1.406(2) Å, whilst the computed bond length gave deviations between 0.001 and 0.015Å from the experimental values.

TABLE 3

*Summary of theoretical and experimental bond lengths (Å), and bond angles (°) for of 2-(4-chlorophenyl)-1H-benzimidazole (**II**) using B3LYP, CAM-B3LYP, B3PW91, WB97XD and M06 functionals and 6-311g(d,p) basis set.*

Bond length (Å) Compound II							
Experimental		B3LYP	B3PW91	WB97XD	M06	Min Deviation	Max Deviation
Cl-C24	1.738(1)	1.673	1.664	1.664	1.664	0.065	0.074
C21-C22	1.390(2)	1.382	1.380	1.384	1.377	0.006	0.013
N1-C1	1.328(2)	1.308	1.306	1.295	1.303	0.020	0.033
N1-C11	1.393(2)	1.390	1.385	1.393	1.379	0.003	0.014
N2-C1	1.362(2)	1.359	1.356	1.344	1.352	0.003	0.018
N2-C12	1.376(2)	1.385	1.380	1.390	1.383	0.004	0.014
C1-C21	1.466(2)	1.477	1.473	1.480	1.472	0.006	0.014
C22-C23	1.381(2)	1.382	1.394	1.384	1.389	0.001	0.013
C11-C12	1.406(2)	1.421	1.419	1.419	1.417	0.011	0.015
Bond Angles (°)							
Experimental		B3LYP	B3PW91	WB97XD	M06	Min Deviation	Max Deviation
C1-N1-C11	104.8(1)	106.4	106.2	106.4	106.2	1.4	1.6
C1-N2-C12	107.2(1)	108.0	108.0	108.1	107.8	0.6	0.9
N1-C1-N2	112.9(1)	110.6	110.7	110.1	110.7	1.9	2.8
N1-C1-C21	125.1(1)	127.4	127.4	127.5	126.9	1.8	2.4
N2-C1-C21	122.0(1)	122.1	122.2	122.4	122.4	0.1	0.4
N1-C11-C16	130.8(1)	128.9	128.8	129.0	128.9	1.8	2.0
N1-C11-C12	109.5(1)	110.6	110.7	110.8	110.7	1.1	1.3
N2-C12-C13	132.0(1)	133.4	133.4	133.2	133.3	1.3	1.4
N2-C12-C11	105.6(1)	104.5	104.5	104.7	104.4	0.9	1.2

The bond lengths of Cl-C24 and C21-C22 were experimentally determined as 1.738(1) and 1.390(2) Å, whilst the computed bond lengths gave deviations between 0.006 and 0.0740 Å from the experimental values. The bond angles of N1-C1-N2, N1-C1-C21, N2-C1-C21 and N1-C11-C16 were experimentally determined as 112.9(1), 125.1(1), 122.0(1) and 130.8(1)° with deviations between 0.1 and 2.8° for the computed values. The bond angles of C1-N1-C11 and C1-N2-C12 were experimentally determined as 104.8(1) and 107.2(1)° with deviations between 0.6 and 1.6° for the computed values. The bond angles of N1-C11-C12, N2-C12-C13 and N2-C12-C11 were experimentally determined as 109.5(1), 132.0(1) and 105.6(1)° with deviations between 0.9 and 1.4° for the computed values. **Figures 3** and **4** gives the crystal packing for compounds **I** and **II.**

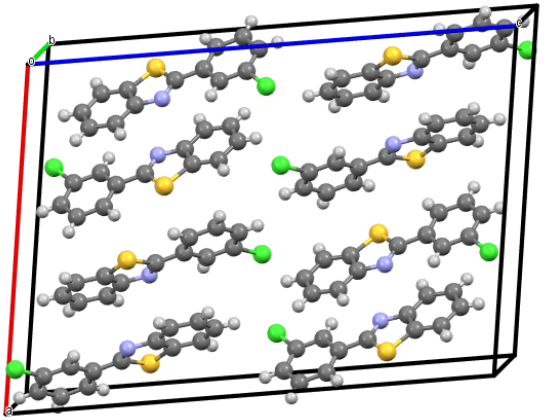


Fig.3: The crystal packing in 2-(3-chlorophenyl)-1,3-benzothiazole **(I)**

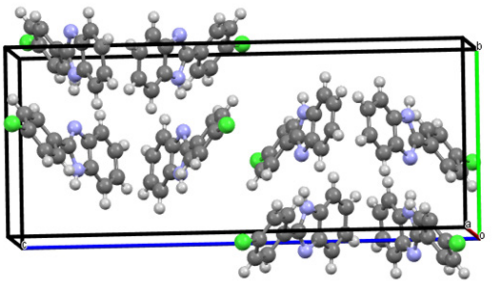


Fig.4: The crystal packing in 2-(4-chlorophenyl)-1H-benzimidazole **(II)**

Hirshfeld surface analysis

Hirshfeld surface analysis is a quantitative way of studying the intermolecular interactions of the molecules in a crystal structure. It gives details of their crystal packing behaviour. Hirshfeld surfaces and fingerprint plots were mapped with Crystal Explorer 3.1 software [19]. The analysis was visualized by the normalized contact distance (dnorm), which was obtained using a high surface resolution with a static colour scale and computed with the equation below.

$$\text{dnorm} = \frac{\text{di} - \text{r}_\text{i}\text{vdw}}{\text{r}_\text{i}\text{vdw}} + \frac{\text{de} - \text{r}_\text{e}\text{vdw}}{\text{r}_\text{e}\text{vdw}}$$

From the equation, *de* is the distance from the Hirshfeld surface to the nearest nucleus outside the surface, *di* is the corresponding distance to the nearest nucleus inside the surface, whilst rvdw is the van der Waals radius/ of the atom [20]. The surface describes the *dnorm* parameter with a red white-blue colour scheme [21]. The bright red spots denotes the intermolecular contacts less than their vdW radii, while the blue spots indicates intermolecular contacts longer than their vdW radii. The white spots are the sum of their vdW radii. Hirshfield surfaces which comprises of *dnorm* surface, shape index and curvedness of compound I was generated using a standard (high) surface resolution as illustrated in **Figure 5**. The *dnorm* surface was mapped on over the range of -0.0365 Å to 1.1265 Å, whilst *di* was mapped over the range of -1.0931 to 2.4756 Å. The parameter *de* was in the range of 1.0961 to 2.5373 Å, the shape index ranging from -1.0000 Å. to 1.0000 Å and curvature lying between -4.0000 Å to 0.4000 Å, whilst the fragment patch was between 0.0000 to 13.0000 Å. For the shape index the red and blue patches confirm the presence of π-π stacking interactions among the aromatic rings in the crystal structure of the compound.

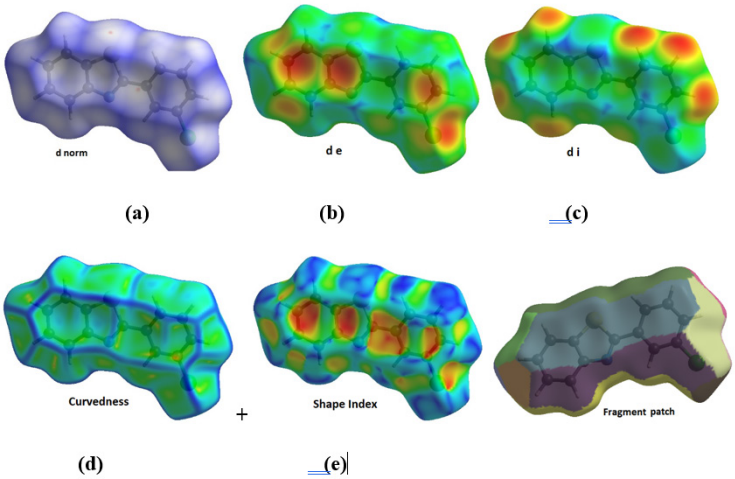


Fig.5: Hirshfeld surfaces mapped for (a) d norm surfaces (b) de surfaces (c) di surfaces (d) shape index (e) curvature and fragment patch of 2-(3-chlorophenyl)-*1H*-benothiazole (**I**).

Figure 6 gives the two-dimensional (2D) fingerprint plots from Hirshfeld surface analyses of compound **I**. It illustrates the relative contribution (in percentage) of the major intermolecular contacts associated with it. The 2D fingerprint plots complement the Hirshfeld surface by providing quantitative information on the nature and type of intermolecular contacts. The most important interaction is H-H which contributes 28.7% to the overall crystal packing. Furthermore, the C-H 26.5%) and Cl-H (18.1%) N-H (4.5%) fingerprint plots also provide information about the intermolecular hydrogen bonds and the contribution of the individual elements towards the crystal packing. H-H interaction (indicated by one spike) is one of the most significant contacts. The fingerprint plot of C-H contacts shows characteristic ‘‘wings’’ which are identified as a result of weak C-H···π interactions. The red triangles on the shape index represented by concave regions indicate π-stacking interactions, whereas the blue triangles represented by convex regions indicate the ring atoms of the molecule inside the surface. The red triangles on the shape index mapping refer to the C-H···π interactions with a contribution of 26.5%, which is in accordance with the 2D fingerprint plot. The curvedness indicates the electron density of surface curves around the molecular interactions. The flat areas of the surface correspond to low value of curvedness, while the sharp curvature area corresponds to high values of curvedness and usually tends to divide the surface into patches, indicating contacts between neighbouring molecules.

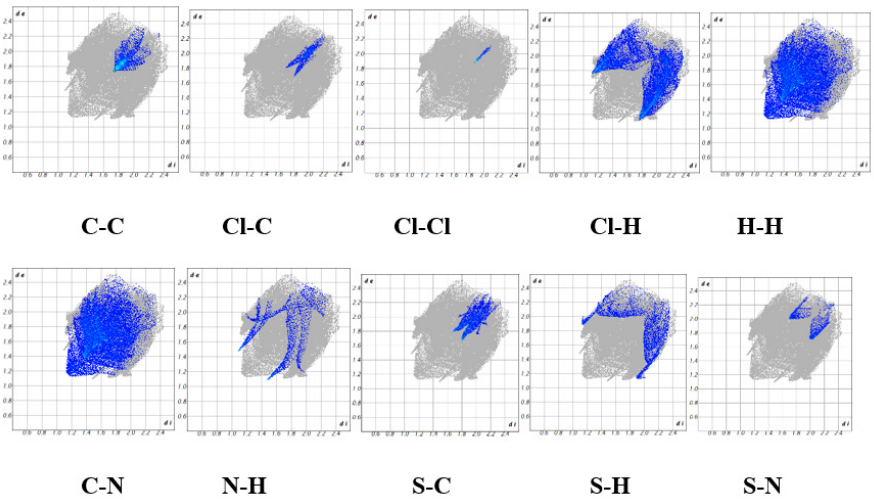


Fig. 6: Relative contributions to the percentage of Hirshfeld surface area for the various intermolecular contacts in 2-(3-chlorophenyl)-1H-benzothiazole **(I)**

The *dnorm* surface, shape index, *di*, *de*, fragment patch and curvedness of compound **II** are provided in **figure 7**. The *dnorm* surface was mapped on over the range of -0.5710 Å to 1.1897 Å, whilst *di* was mapped over the range of 0.7562 to 2.5256 Å. The parameter *de* was in the range of 0.7552 to 2.5371 Å, the shape index ranging from -1.0000 Å. to 1.0000 Å and curvature lying between -4.0000 Å to 0.4000 Å, whilst the fragment patch was between 0.0000 to 15.0000 Å.

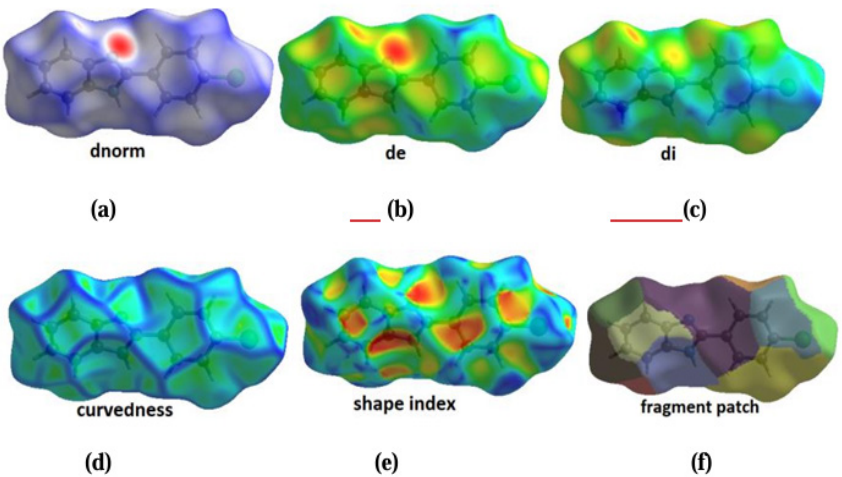


Fig.7: Hirshfeld surfaces mapped for (a) d norm surfaces (b) de surfaces (c) di surfaces (d) shape index and (e) curvature (f) fragment patch of 2-(4-chlorophenyl)-*1H*-benzimidazole **(II)**.

Figure 8 gives the two-dimensional (2D) fingerprint plots from Hirshfeld surface analysis of compound **II**. It illustrates the relative contribution (in percentage) of the major intermolecular contacts associated with it. The 2D fingerprint plots has been provided to complement the Hirshfeld surface analysis. It provides quantitative information on the nature and type of intermolecular contacts. H-H contributes 34.5% to the overall crystal packing, with C-H (30.1%), Cl-H (12.5%) and N-H (10.2%). The fingerprint plots provides information about the intermolecular hydrogen bonds and the contribution of the individual elements towards the crystal packing. H-H interaction is one of the most significant contacts. The fingerprint plot of C-H contacts shows characteristic ‘‘wings’’ which are identified as a result of weak C-H···π interactions. There are minor contributions from Cl-C (4.1%), Cl-N (1.9%) and Cl-Cl (2.1%) to the surface maps of the compound. The curvedness indicates the electron density of surface curves around the molecular interactions.

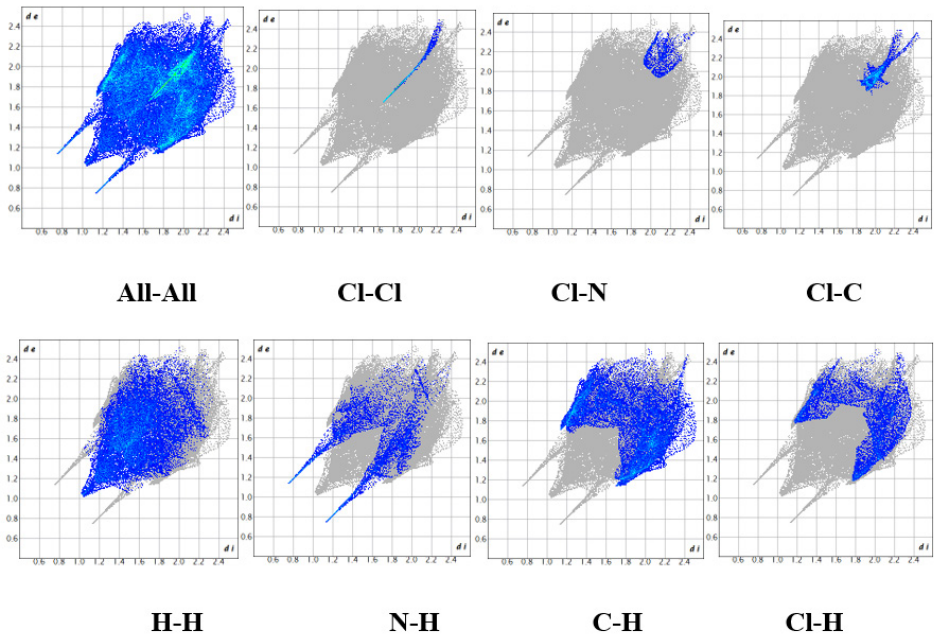


Fig.8: Relative contributions to the percentage of Hirshfeld surface area for the various intermolecular contacts in 2-(4-chlorophenyl)-1H-benzimidazole **(II).**

HOMO–LUMO analysis

Chemical stability of any species can be predicted with the help of the HOMO and LUMO [22, 23], the ability to accept an electron is defined by the LUMO whilst the ability to donate an electron described by the HOMO. The ionization potential is determined by the HOMO whilst the electron affinity depends on the LUMO. The energy of the HOMO decides the ionization potential whilst the

energy of the LUMO determines the electron affinity. The HOMO-LUMO energy gap indicates the stability, reactivity and the electrical conductivity of the molecules [24, 25]. A lower energy gap corresponds to a higher conductivity and vice versa. The hardness of a molecule also depends on the magnitude of the HOMO-LUMO gap [26]. Chemical reactivity and kinetic stability of the molecule can be characterized using the energy gap [27]. The energies of frontier molecular orbitals, energy band gap (E_{HOMO}-E_{LUMO}), electronegativity (χ), chemical potential (μ), global hardness (η), global softness (S) and global electrophilicity index (ω) all contribute to the reactivity of the molecule concerned. Kinetic stability of molecules have been reported to be related to hardness [28]. The electrophilicity index enables the quantitative classification of the global electrophilic nature of a molecule within a relative scale [29-31]. The HOMO–LUMO energy levels and plots of compounds **I** and **II** using B3LYP, B3PW91, WB97XD and M06 functionals and 6-311++G (3df, 3pd) basis sets are provided in **Tables 4, 5, S1** and **S2**. The HOMO and LUMO for the compound **I** gave energy gaps between 0.04428 and 0.16538 eV, whilst the HOMO-LUMO gap for compound **II** was between 0.06639 to 0.19189 eV [32].

TABLE 4

*HOMO–LUMO energy levels of 2-(4-chlorophenyl)-1, 3-benzimidazole **(I)** using B3LYP, B3PW91, WB97XD and M06.*

	Compound I			
Energy levels	**B3LYP**	**B3PW91**	**WB97XD**	**M06**
LUMO+4	-0.30824	-0.30961	-0.23058	-0.29882
LUMO+3	-0.31100	-0.31213	-0.23825	-0.30243
LUMO+2	-0.31953	-0.32092	-0.25028	-0.31198
LUMO+1	-0.38997	-0.39114	-0.32610	-0.38170
LUMO	-0.49076	-0.49407	-0.43617	-0.48436
HOMO	-0.53504	-0.53795	-0.60155	-0.54198
HOMO-1	-0.54977	-0.55274	-0.62519	-0.55909
HOMO-2	-0.57321	-576761	-0.64463	-0.58128
HOMO-3	-0.58343	-0.58718	-065136	-0.59039
HOMO-4	-0.60262	-0.60414	-0.68895	-0.61415
HOMO-LUMO GAP (eV)	0.04428	0.04388	0.16538	0.05762

TABLE 5

*HOMO–LUMO energy levels of 2-(3-chlorophenyl)-1H-benzothiazole **(II)** using B3LYP, B3PW91, WB97XD and M06 functionals and 6-311++G (3df, 3pd) basis* set.

	Compound 1I			
Energy levels	**B3LYP**	**B3PW91**	**WB97XD**	**M06**
LUMO+4	-0.29137	-0.29214	-0.21739	-0.28326
LUMO+3	-0.30104	-0.30195	-0.22530	-0.29264
LUMO+2	-0.31363	-0.31481	-0.23894	-0.30563
LUMO+1	-0.37277	-0.37396	-0.30633	-0.36492
LUMO	-0.47563	-0.47849	-0.42044	-0.46943
HOMO	-0.54211	-0.54488	-0.61233	-0.55267
HOMO-1	-0.56007	-0.56302	-0.62617	-0.56677
HOMO-2	-0.57084	-0.57423	-0.64712	-0.58021
HOMO-3	-0.59295	-0.59509	-0.67009	-0.60205
HOMO-4	-0.59986	-0.60131	-0.68423	-0.61219
HOMO-LUMO GAP (eV)	0.06648	0.06639	0.19189	0.08324

Conclusions

The study confirms the successful synthesis of 3-chlorophenyl benzothiazole and 4-chlorophenyl benzimidazole *via* Bismuth nitrate catalysis. The compounds were characterized using Infra-red spectroscopy, Nuclear Magnetic Resonance Spectroscopy, microanalysis and Gas Chromatography-Mass Spectrometry. The X-ray diffraction studies showed that compound **I** crystallized in the Monoclinic *I2/a* and whilst compound *II* crystalised in the orthorhombic *Pbca*, with eight molecules each in the unit cell held together Van der Waals interaction. The crystal packing for compound *I* showed that the contributions came from H···H (28.7%), H···C/C···H (26.5%), Cl···H (18.1%) and H···N/N···H (4.5%) whilst the crystal packing in compound II were from H···H (34.5%), H···C/C···H (30.1%), Cl···H (12.5%) , H···N/N···H (10.2%), Cl···C (4.1%), Cl···N (1.9%) and Cl···Cl (2.1%).

Acknowledgements

We are also grateful for the helpful support of CHPC (www.chpc.ac.za) (CHEM1260)

Additional information

CCDC 1528309 and 1528306 contain the supplementary crystallographic data for this paper. These data can be obtained free of charge via http://www.ccdc.cam.ac.uk/conts/retrieving.html (or from the Cambridge Crystallographic Data Centre, 12, Union Road, Cambridge CB2 1EZ, UK; fax: +44 1223 336033).

Data availability:

Data are available on the main manuscript and supplementary materials

References

ÖZKAY, Y., TUNALI, Y., KARACA, H. & SIKAG, I. Antimicrobial Activity and a SAR Study of Some Novel Benzimidazole Derivatives Bearing Hydrazone Moiety. European Journal of Medicinal Chemistry **45**, (2010) 3293−3298.

PATEL, V. M., PATEL, N. B., CHAN-BACAB, M. J., RIVERA, G. N-Mannich Bases of Benzimidazole as a Potent Antitubercular and Antiprotozoal Agents: Their Synthesis and Computational Studies, Synthetic Communications **50**, (2020) 858−878.

KÜÇÜKBAY, H. Part I: Microwave-assisted synthesis of benzimidazoles: An overview (until 2013), Journal of the Turkish Chemical Society Section A: Chemistry, 4, (2017) 1−22TATAR, E., KARAKUS, S., KŰĆŰKGŰEL, Ş. G., OKULLUU, S. Ő., ÜNŰBOL, N., KOCAGŌZ, T., De CLERCQ, E., ANDREI, G., SNOECK, R., PANNECOUQUE, C., KALAY, S., ŞAHIN, F., SRIRAM, D., YOGEESWARI, P., KŰĆŰKGŰREL, I. Design, Synthesis, and Molecular Docking Studies of a Conjugated Thiadiazole–Thiourea Scaffold as Antituberculosis Agents, Biological and Pharmaceutical Bulletin, **39**, (2016) 502–515.

CHEN, W., LIA, K., WANG, Y. & XIA, Z., Microwave-assisted synthesis of benzothiazole urea derivatives, Journal of Chemical Research. (2010) 75–79.

SALLAM, H. H., MOHAMMED, Y. H. I., Al-OSTOOT, F. H., AKHILESHWARI, P., M. A. SRIDHAR, M. A. & KHANUM, S. A. Experimental and computational studies on the synthesis and structural characterization of 2-(4-chlorophenoxy)-N-[4-(4-methylphenyl)-1,3-thiazol-2-yl]acetamide, Journal of Molecular Structure, **1249**, (2022) 131588.

CELIK, I., ÇEVIK, U. A., KARAYEL, A., ISAK, A., KAYIŞ, U., GÜL, U. D., BOSTANCI, H. E., KONCA S. F., ÖZKAY, Y. &

KAPLANCIKLI, Z.A. Synthesis, Molecular Docking, Dynamics, Quantum-Chemical Computation, and Antimicrobial Activity Studies of Some New Benzimidazole–Thiadiazole Hybrids, ACS Omega **7** (2022) 47015−47030.

CAN, N. Ö., ÇEVIK, U. A., SAĞHK, B. N., LEVENT, S., B. KORKUT, Y. ÖZKAY, KAPLANCIKH, Z. A. & KOPARAL, A. S., (2017). Synthesis, molecular docking studies, and antifungal activity evaluation of new benzimidazole-triazoles as potential lanosterol 14 α-demethylase inhibitors, Journal of Chemistry, **15**, ID 9387102,

PARDESHI, S. D., SONAR, J. P., PAWAR, S. S., DEKHANE, D., GUPTA, S., ZINE, A. M. & THORE, S. N. Journal of the Chilean Chemical Society, **59**, (2014) 2335−2340.

El-ARAB, E. E., El-SAID, A. I., AMINE, M. S. & MOHARRAM, H. H. Synthesis and Antitumor Activity Evaluation of New 2-(4-aminophenyl) benzothiazole/oxazole/ imidazole Derivatives, Egyptian. Journal of Chemistry, **59** (2016) 967− 984.

CHAUHAN, K., CHOUDHARY, D., KUMAR, A., DHIMAN, S., JAMWAL, S., DHAIYA, D. P. & CHAUDHARY, A. World Journal of Pharmaceutical and life sciences, **5**, (2019) 108−115.

APEX2 SADABS and SAINT. Bruker AXS Inc: Madison, WI, USA. 2010.

SHELDRICK, G.M., A Short History of SHELX. Acta. Cryst A. 64, (2008) 112−122.

HUBSCHLE, C. B., SHEDRICK, G. M. & DITTRICH, B. (2011) ShelXle: A Qt Graphical User Interface for SHELXL, Journal of Applied Crystallography, **44**, 1281.

ODAME, F., KLEYI, P., HOSTEN, E. C., BETZ, R., LOBB, K. & TSHENTU, Z. R. (2013) The Formation of 2,2,4-Trimethyl-2,3-dihydro-1H-1,5-Benzodiazepine form 1,2-Diaminobenzene in the Presence of Acetone, Molecules **18**, 14293–14305.

ODAME, F., HOSTEN, E., BETZ, R., LOBB, K. & TSHENTU, Z. (2015) Benzimidazole or Diamide from a reaction of Diamides and Carboxylic Acids or Acid Chlorides: Crystal structures and Theoretical studies, Acta Chimica Slovenica, **62**, 986−994.

ODAME, F., SCHOEMAN, R., KRAUSE, J., HOSTEN, E. C., TSHENTU, Z. R. & FROST, C. L. (2021) Synthesis, characterization, crystal structures, and anticancer activity of some new 2,3-dihydro-1,5-benzoxazepines, Medicinal Chemistry Research, **30**, 987–1004.

ODAME, F., HOSTEN, E. C., BETZ, R., KRAUSE, J., FROST, C. L., LOBB, K. & TSHENTU, Z. R. (2021) Synthesis, characterization, computational studies and DPPH scavenging activity of some triazatetracyclic derivatives, Journal of the Iranian Chemistry Society, **18**, 1979–1995.

WOLFF, S. K., GRIMWOOD, D. J., MCKINNON, J. J., TURNER, M. J., JAYATILAKA D., & SPACKMAN, M. A. Crystal Explorer 3.0. University of Western Australia, Perth, (2012).

ELTAYEB, N. E., ŞEN, F., LASRI, J., HUSSIEN, M. A., ELSILK, S. E., BABGI, B. A., GÖKCE, H. & SERT, Y. (2020). Hirshfeld Surface analysis, spectroscopic, biological studies and molecular docking of (4E)-4-((naphthalen-2-yl)methyleneamino)-1,2-dihydro-2,3-dimethyl-1-phenylpyrazol-5-one, Journal of Molecular Structure, **1202**, 127315.

SPACKMAN, M. A. & JAYATILAKA, D. Hirshfeld surface analysis, Crystal Engineering Communications, **11**, (2009). 19–32.

SARALA, S., GEETHA, S. K., MUTHA, S. & IRFAN, A. Computational investigation, comparative approaches, molecular structural,

vibrational spectral, non-covalent interaction (NCI), and electron excitations analysis of benzodiazepine derivatives, Journal of Molecular Modeling **27**, (2021) 266.

CHOUDHARY, V., BHATT, A., DASH, D. & SHARMA, N. DFT Calculations on Molecular Structures, HOMO–LUMO Study, Reactivity Descriptors and Spectral Analyses of Newly Synthesized Diorganotin (IV) 2-Chloridophenylacetohydroxamate Complexes, Journal of Computational Chemistry, **40**, (2019) 2354−2363.

MATUNOVÁ, P., JIRAŞEK, V. & REZEK, B. (2019) DFT calculations reveal pronounced HOMO–LUMO spatial separation in polypyrrole–nanodiamond systems, Physical Chemistry Chemical Physics, **21**, 11033−11042.

PADMAJA, L., KUNAR, R. C., SAJAN, D., JOE, I. H., JAYAKUNMAR, V. S., PETTIT, G. R. & NIELSEN, O. F. (2009) Density functional study on the structural conformations and intramolecular charge transfer from the vibrational spectra of the anticancer drug combretastatin-A2, Journal of Raman Spectroscopy **40**, 419–428.

POIYAMOZHI, A., SUNDARAGANESAN, N., KARABACAK, M., TANRIVERDI, O. & KURT, M. (2012) The spectroscopic (FTIR, FT-Raman, UV and NMR), first-order hyperpolarizability and HOMO–LUMO analysis of 4-amino-5-chloro-2-methoxybenzoic acid, Journal of Molecular Structure **1024**, 1–12.

UDAYAKALA, P., JAYANTHI, A., RAJENDIRAN, T.V. & GUNASEKARAM, S. Molecular structure, FT-IR and FT-Raman spectra and HOMO-LUMO analysis of 2-methoxy-4-nitroaniline using ab initio HF and DFT (B3LYP/B3PW91) calculations, Archives of Applied Science Research **3**, (2011) 424–439.

GOVINDARAJAN, M., PERIANDY, S. and CATHIGAYEN, K. FT-IR and FT-Raman spectra, thermo dynamical behavior, HOMO and LUMO, UV, NLO properties, computed frequency estimation analysis and electronic structure calculations on α-bromotoluene, Spectrochimica Acta A, **97**(2012) 411– 422.

PARR, R. G., CHATTARAJ, P. K. Principle of maximum hardness, Journal of the American Chemical Society, **113**, (1991) 1854–1855.

PARR, R. G., SZENTPALY, L. V. and LIU, S. Electrophilicity Index, Journal of the American Chemistry Society, **121**, (1999) 1922–1924.

PARTHASARATHI, R., PADMANABHAN, J., SUBRAMANIAN, V., MAITI, B. & CHATTARAJ, P. K. (2003) Chemical Reactivity Profiles of Two Selected Polychlorinated Biphenyls, Journal of Physical Chemical A 107, 10346–10352.

PARTHASARATHI, R., PADMANABHAN, J., SUBRAMANIAN, V., MAITI, B., CHATTARAJ, P. K. Toxicity analysis of 33'44'5 – Pentachloro Biphenyl Through Chemical Reactivity and Selectivity Profiles, (2004) Current Science, **86**, 535–542.

Received 25 Nov. 25; revised 25 Jun. 26.